Journal of Biomechanical Engineering. Received August 09, 2020;
Accepted manuscript posted May 11, 2021. doi:10.1115/1.4051116

A novel *in vitro* and *in silico* system for analysing complex mechanobiological behaviour of chondrocytes in 3D hydrogel constructs

Authors: Sophia Leung[1], Jung-Joo Kim[2], David S Musson[3], Sue R McGlashan[4], Jillian Cornish[3], Iain Anderson[1] and Vickie B.K. Shim[1]

Affiliations:

1. Auckland Bioengineering Institute, University of Auckland, New Zealand
2. Department of Biomedical Science, Biomedical Science and Engineering, Inha University College of Medicine, South Korea
3. Department of Medicine, Faculty of Medical and Health Sciences, University of Auckland, New Zealand
4. Department of Anatomy and Medical Imaging, Faculty of Medical and Health Sciences, University of Auckland, New Zealand

Corresponding author: Vickie Bo Kyung Shim

Mailing Address:
Auckland Bioengineering Institute, University of Auckland
Level 6, 70 Symonds Street
Auckland 1010
New Zealand
Email: v.shim@auckland.ac.nz

Abstract

Physiological loading is essential for the maintenance of articular cartilage through regulation of tissue remodelling. To correctly understand the behaviour of chondrocytes in their native environment, cell stimulating devices and bioreactors have been developed to examine the effect of mechanical stimuli on chondrocytes. The current study describes the design and validation of a novel system for analysing chondrocyte deformation patterns. This involves an *in vitro* mechanical device for a controlled application of multiaxial-loading regimes to chondrocyte-seeded agarose constructs and *in silico models* for analysing chondrocyte deformation patterns.

The computer-controlled device precisely applies compressive, tensile and shear strains to hydrogel constructs using a customisable macro-based programme. The synchronisation of the displacements is shown to be accurate with a 1.2% error and is highly reproducible. The device design allows housing for up to 8 novel designed free-swelling 3D hydrogel constructs. Constructs include mesh ends and optimised to withstand the application of up to 7% mechanical tensile and 15% shear strains. Constructs were characterised through mapping the strain within as mechanical load was applied and was validated using light microscopy methods, chondrocyte viability using live/dead imaging and cell deformation strains. Images were then analysed to determine the complex deformation strain patterns of chondrocytes under a range of dynamic mechanical stimulations.

This is one of the first systems that have characterised construct strains to cellular strains. The features in this device make the system ideally suited for a systematic approach for investigation of the response of chondrocytes to a complex physiologically relevant deformation profile.

Introduction

Articular cartilage functions as a shock absorber and load distributer at the weight bearing interfaces within synovial joints. Its unique material properties withstand a wide range of mechanical demands and provide smooth articulation. It is well established that physiological loading is essential for the maintenance of the articular cartilage [1–3], which is exposed daily to a combination of complex strains such as compression, tension, and shear [2,4–6].

Due to the limited capacity to regenerate and to repair itself, damage to the articular cartilage is often irreversible and progressive. Therefore, numerous *in vitro* models have applied mechanical conditioning devices to *in vitro* models to mimic the *in vivo* environment of cartilage [7–12] in order to better understand and mitigate the progressive degeneration of articular cartilage, or to engineer neo-cartilage. Whereas many of these devices are limited to the application of uniaxial loads (compression, 2D tension, or shear), the cells of cartilage, known as chondrocytes, are exposed to multi-axial forces *in vivo*; therefore, these devices have restricted capability to simulate the complex physiological loading environment of cartilage.

Recently, several devices have been developed to apply multi-axial loading to chondrocytes *in vitro*, such as combining compression and topological shear loading [13–16]. While these devices have provided the ability to apply multi-axial forces to cells *in vitro*, the applied stimuli are not independently controlled and often do not include tensile strain, which is also experienced by cartilage [17–19]. There have also been several limitations in current mechanical compression conditioning devices, such as viscoelastic relaxation of hydrogel samples over time due to gravity, attachment of hydrogels to mechanical devices, as well as limitations in measuring the transferred mechanical load to the samples and cells. Developing a bioreactor that can overcome these design limitations and closely mimics mechanical forces present *in vivo* will enable more accurate development of *in vitro* models to be used for the study of cartilage, with the potential to produce neo-cartilage possessing properties closely matching that of native tissue.

The current study aimed to develop a device that included controlled combinations of dynamic compression, tension and shear strain loading of chondrocyte seeded hydrogels to closely mimic the complex *in vivo* conditions of the knee. One of the key measures in analysing chondrocyte behaviour under different mechanical loads is morphological changes, which are known to influence gene expression and chondrocyte metabolism [8,20,21]. This study presents the design and validation of a novel mechanical loading device that applied complex mechanical loads to an *in vitro* cell model and coupled the morphological data to *in silico* cell models capable of accurately measuring cell morphological changes and cellular strains during mechanical stimulation.

Journal of Biomechanical Engineering. Received August 09, 2020;
Accepted manuscript posted May 11, 2021. doi:10.1115/1.4051116

Materials and Methods

We set several design criteria that the device and constructs had to overcome limitations in the literature. 1) The device was to ensure that a wide range of compressive, tensile and mechanical shear dynamic loading could be applied individually and simultaneously to cells cultured in 3D hydrogel. The percentage strain range to be achieved was between 0-20% with a loading frequency of at least 1 Hz to represent physiologically normal loading, but to allow for modifications in loading patterns that could also represent abnormal mechanical loading; 2) Multiple samples were to be dynamically loaded at one time to enable different assays to be carried out from one experiment; 3) Stress relaxation of hydrogel samples should be minimized; 4) Cells should be able to be imaged under dynamic loading.

Design of a multi-axial device

The overall system is aligned horizontally and composed of three main platforms: a top platform, a middle platform, and a baseplate, as shown in Fig. 1 A. The different platforms enable individual and simultaneous operation of the actuators.

The loading system provides compressive and tensile strain via linear actuators (M-229.26S, Physik Instrumente, Karlsruhe, Germany) mounted on the top platforms, in parallel to the constructs. The M-229.26S linear actuators have a positioning accuracy of 0.078 µm, and a maximum speed of 5 mm/ s. The actuator shaft is connected to an arm, which acts as the loading platen indicated in Fig. 1 B. Constructs are attached to the loading platen and central bar, so that mechanical load is applied in the horizontal plane. Two linear slide units (BMU 12-30, IKO, Tokyo, Japan) on each side of the top platform guide the movement of the loading platen.

Shear strains are provided via two smaller linear actuators (M-228.11S, Physik Instrumente, Karlsruhe, Germany) mounted on the middle platform perpendicular to the constructs, with the same accuracy and speed capabilities as the M-229.26S. These actuator shafts are connected to the top platform via the platform arms.

Four small linear actuators (PQ12-100-6-S, Firgelli Technologies, CA) are also mounted on the middle platform with the pusher-shaft attached to the baseplate. During extension, it raises the top and middle platforms so that the samples in the 8-well culture plate sitting in the plate carrier can slide into position (Fig. 1 B).

Journal of Biomechanical Engineering. Received August 09, 2020;
Accepted manuscript posted May 11, 2021. doi:10.1115/1.4051116

Top and middle platforms, central bar, loading platens, and platform arms were constructed with standard 6061 aluminium alloy, and then anodized. All surfaces of the device were able to be sterilised with 70% ethanol.

Control System. Each of the M-229.26S and M-228.11S actuators is connected to its own controller (C-663 Mercury™, Physik Instrumente, Karlsruhe, GE), which enables either simultaneous or independent control of the actuators via the PIMikroMove™ software. Custom macro command scripts were written and implemented in the software to generate a various waveforms, such as continuous sinusoidal loading or programmable loading patterns with periods of unloading, strain amplitudes (between 0-20% strain) and frequencies (variable between 0.5- 2 Hz).

Assessment of the accuracy of mechanical loading

To ensure the accuracy and reproducibility of the device, a validation protocol examined the movement of the loading platens in the parallel (compression and tension) and perpendicular (shear) direction. The displacement and waveform of the loading platens in each direction was monitored using a laser displacement meter (LC-2440 Keyence, Tokyo, Japan) and Labview (LabView version 2013, National Instruments, USA), see appendix Fig. S1. The actuators were prescribed to move sinusoidally between the starting and target displacement (within the range of 0 and 2.25 mm, equivalent to 2%, 4%,

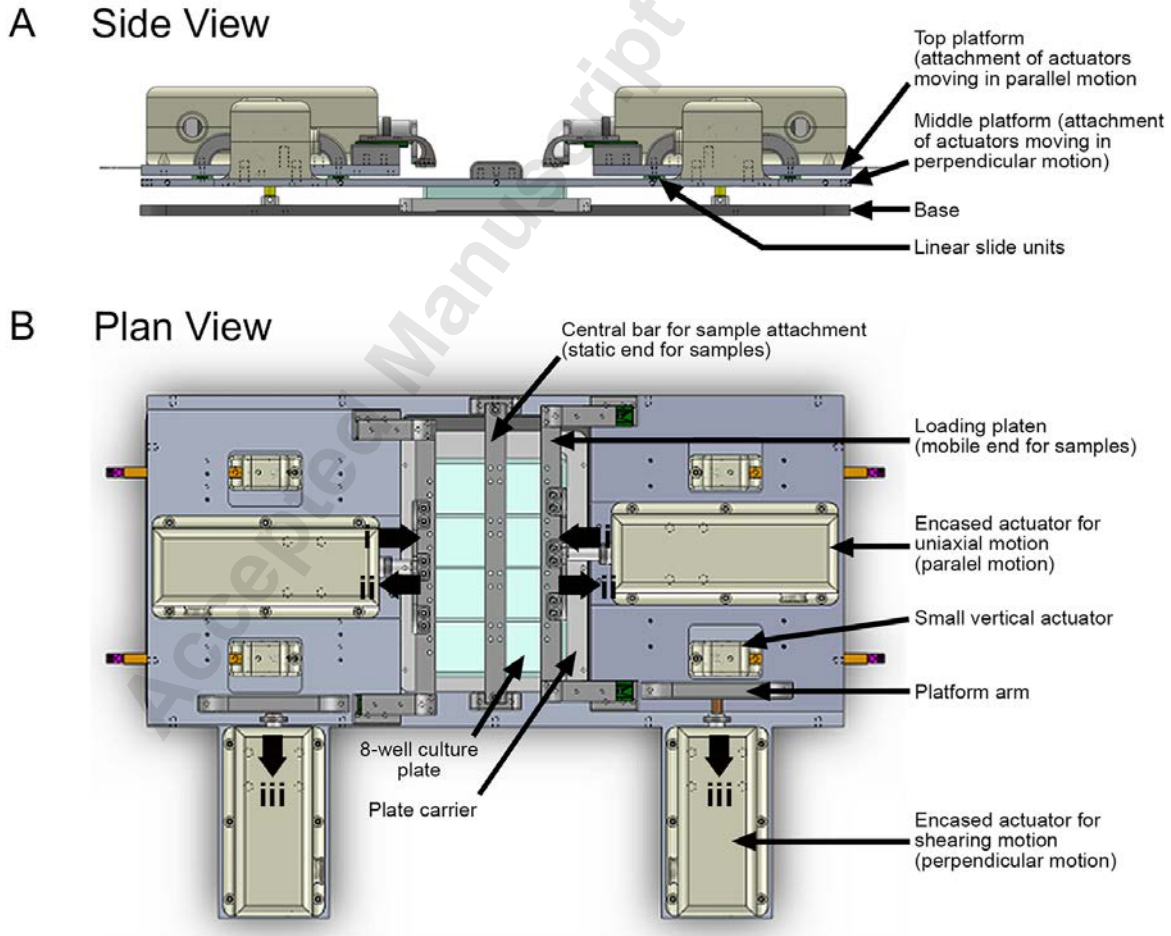

Figure 1. Schematic of assembled device in (**A**) side and (**B**) plan view. The side view shows the device in the raised state. Thick black arrows indicate actuators movement direction to apply (i) compressive, (ii) tensile and (iii) shear strains.

6%, 8%, 10%, 12%, and 15% applied uniaxial strain on constructs) at a frequency of 1 Hz for one minute. Each displacement profile was repeated three times and averaged to calculate the percentage error.

Construct design, fabrication and cell culture

A rectangular construct was developed as shown in Fig. 2 A. The construct design involves two mesh-rigid ends. Epoxy designed for medical use for adhesion to metals and plastics (Polytec EP 601-T, Polymere Technologien, Waldbronn, Germany) was used to bond evenly spaced stainless steel mesh (34 mesh 0.065", grade 316, TWP, CA, USA) inserts into rigid end plates, which were 3D printed using the stereolithography (SLA) process with material (WaterShed® XC 11122, DSM Somos, IL, USA) that passed International Organization for Standardisation biocompatibility tests (ISO 10993). Cell-seeded molten hydrogel infiltrates the pores of the mesh, and upon gelation, attach to the rigid end plates, which enable the constructs to attach to the device. The dimensions of the hydrogel (15 x 13 x 3 mm) were optimised to prevent buckling during compression, while the mesh type was optimised to increase the contact between the cell-seeded hydrogel and the rigid ends. The mesh type was also optimised to enable maximum tensile strain range, see supplementary Fig. S2. The mesh-rigid ends attach the constructs to the centre bar and the loading platen of the device with M2.5 threaded screws as shown in Fig. 2 B.

Construct Preparation and Culture Conditions.

An immortalised mouse articular chondrocyte cell line (H5 clone, a gift from P.M. van der Kraan and H.M. van Beuningen, Radboud University Medical Center, Nijmegen, The Netherlands) [22] was cultured in a T75 flask in Dulbecco's Modified Eagle's Medium (DMEM) containing 10% foetal bovine serum (FBS), and 0.1% penicillin/ streptomycin (Life Technologies Ltd, NZ) at 37°C/5% CO_2 until 90% confluent. Cells were trypisined, counted and assessed for viability using the trypan blue exclusion assay, then re-suspended in fresh medium at a concentration of 8×10^6 cells/ml. The chondrocyte suspension was mixed with an equal volume of autoclaved 6% (w/v) agarose (type VII, Sigma-Aldrich, Missouri, USA) to give a final concentration of 4×10^6 cells/ml in 3% agarose gel.

The chondrocyte-agarose suspension was pipetted into sterilized rectangular shaped acrylic moulds containing the mesh-rigid ends, also sterilized, described above. Chondrocyte-agarose gels were set at 4°C for 20 minutes. The resulting chondrocyte-agarose constructs were removed from the moulds, and maintained in seeding medium DMEM, 10% FBS, and 20 μg/ml L-ascorbic acid 2-phosphate (AA2P, Sigma-Aldrich, MO, USA) in 8-well culture plates (Greiner Bio-One, Medi'Ray, NZ). Chondrocyte-agarose constructs were cultured in 37 ˚C/5% CO_2 for 14 days, media was changed every 1 to 2 days. Mechanical loading was carried out on day 15. For construct strain validation experiments, carbon dust was added to a subset of chondrocyte-agarose suspension samples at the end of the 14 day culture period prior to the application

of mechanical strain. Three constructs on one side of the device was used to apply one type of strain, with one sample detached from the device to use as unloaded control. The other side of the device was used to apply a separate strain type, with an internal control.

Construct Characterization with Applied Dynamic Loading

Construct and cell strain were analysed on samples under compressive, tensile and shear strains only. This enabled a better understanding of how each of these strains affect the construct and cell individually. However, to assess cell viability after loading, all loading regimes were used.

Construct Strain

At the end of the 14 day culture period, either compressive, tensile or shear strains were applied to chondrocyte-agarose constructs to determine the correlation between applied dynamic strains and the engineering strains within each construct. Dynamic strains through the construct were measured by adding carbon dust (Electroflash Resourcing Ltd, NZ) during construct preparation, as previously detailed in [23]. The construct was attached to the device, which was secured on a lighting stage with a Sony NEX-5 camera with macro fitted Voigtänder 40 mm f/1.4 x NOKTON Classic lens, mounted directly above it, and images of the whole construct were captured at 3344×2224 pixels. Constructs were then subjected to either compressive, tensile or shear strain load at a loading rate of 20 µm/ s. The maximum dynamic strain applied to

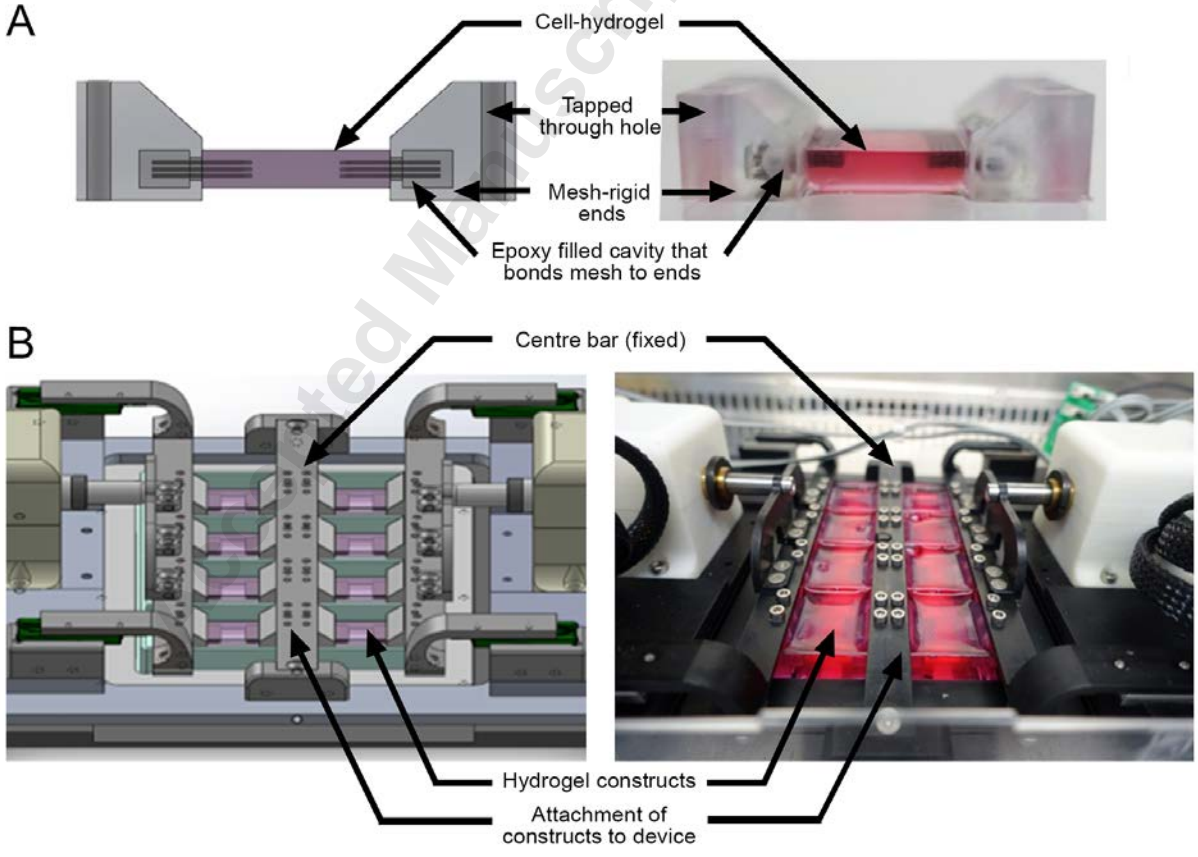

Figure 2. (**A**) Side view of assembled construct in (*left*) schematic and (*right*) image. (**B**) Samples attached to the device in (*left*) schematic and (*right)* image.

constructs were 15% for compression, 7% for tension, and 15% for shear strains. Free-swelling (unloaded) constructs acted as controls and were imaged in an identical manner.

Images were analysed using a MATLAB program developed and validated by Malcom et al [24,25], which we have used previously to characterize 3D strain fields within hydrogels [23]. Briefly, the program applied a grid map to the reference image (uncompressed). Each pixel was then traced in the sequential images through the compression of the gel using a cross-correlation technique. The carbon powder created a unique arrangement that allowed its movement to be tracked and coordinates saved. To measure the strain distribution in the gel during compression, each image was compared to the reference image, and the engineering strain between each data point within the image was calculated. The engineering strain refers to the difference of the co-ordinate displacement between the new image and the reference image, divided by the original position of the reference image. The strains measured in the direction of applied load (X direction) were termed the 'reported strains'. The strain values were plotted to their associated coordinate along the length of the construct, relative to the fixed end of the construct, using CMISS (open source software for computational biomechanics developed by the Auckland Bioengineering Institute; www.cmiss.org). Three samples were measured for each compression, tensile and shear loads. The immobile end of the construct attached to the central bar of the device is herein termed the "fixed end"; the other end of the construct attached to the loading platen where load is applied by the device is herein termed the "mobile end".

Cell Strain

To determine the correlation between applied strain and cellular strains, constructs were attached to the device, and the system was mounted on an inverted microscope (Nikon TE2000E Inverted Microscope). The same loading conditions as described for construct strain were applied to the chondrocyte-agarose constructs following 14 days in free-swelling culture. Cells were imaged using Image Pro Plus (version 7.1, MediaCybernetics) using a 40 X/0.4 NA objective lens with Hoffman modulation contrast mode. The centre of the construct was imaged each time for consistency. Compression, tensile or shear strain was applied at 20 μm/ s, and cells under deformation were captured at 0.5% applied strain increments. Free-swelling (unloaded) constructs acted as controls and were imaged in an identical manner.

Each image set was subjected to image processing using NIH ImageJ software (http://rsb.info.nih.gov/ij/)"; a pseudo flat field correction was applied with a blurring radius of 5 pixels to remove out-of-focus cells, while flattening the background. The Cell Magic Wand toolbox was used to draw the boundaries of individual cells within the field of view, as shown in Fig. 3, and the positions were stored in order to identify the same set of cells in each image set. Ten cells per construct were measured for each of the loading conditions, and all experiments were performed in triplicate.

The cell strain in the direction of applied load was calculated in the form of Lagrangian strain using the theory of finite deformation elasticity [26]. The deformation of the cell shape was measured by first fitting a 2D mesh comprising four-noded rectangular elements to the cell boundaries obtained from cell images (Fig. 3). Then this was morphed to the deformed cell shape using the least-square fitting method [27] The strain between original and deformed meshes was computed using the deformation gradient tensor between the two, which was quantified by measuring the change in length of material segments. Given a material vector in the undeformed state (d**X**) which is mapped to the deformed state (d**x**), the gradient deformation tensor (F) was defined as the following Eq. (1):

$$\mathbf{F} = \frac{d\boldsymbol{x}}{d\boldsymbol{X}} \tag{1}$$

Strain in a deformed mesh is determined by measuring segment length changes, by computing the square length (ds^2) for the deformed segment d**x** giving Eq. (2),

$$ds^2 = dx^i x^i = d\boldsymbol{x}^T d\boldsymbol{x} = (\boldsymbol{F}d\boldsymbol{X})^{\boldsymbol{T}}\boldsymbol{F}d\boldsymbol{X} = d\boldsymbol{X}^T\boldsymbol{F}^T\boldsymbol{F}d\boldsymbol{X} = d\boldsymbol{X}^T\boldsymbol{C}d\boldsymbol{X} \tag{2}$$

From this we calculated the Cauchy-Green deformation tensor:

$$\boldsymbol{C} = \boldsymbol{F}^T\boldsymbol{F} \tag{3}$$

Finally, using the deformation Eq. (3) we derived the Lagrangian finite strain tensor:

$$\boldsymbol{E} = \frac{(\boldsymbol{C} - \boldsymbol{I})}{2} \tag{4}$$

The cell deformation and surface strain patterns in chondrocytes after mechanical loading was described with the final Lagrangian strain tensor Eq. (4).

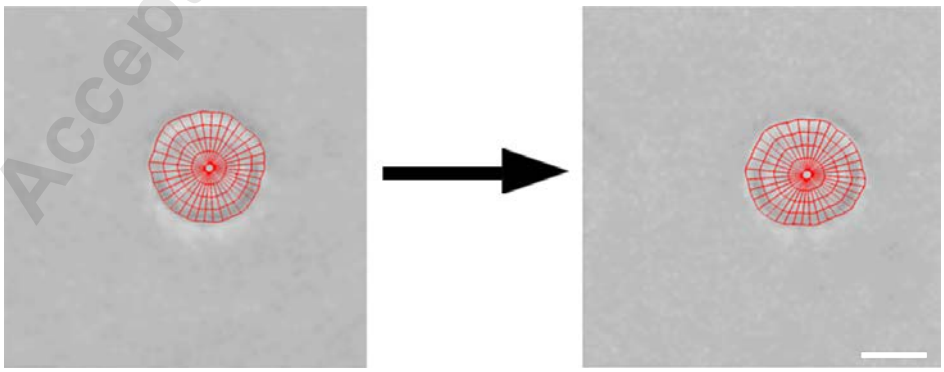

Figure 3. Representative of fitting a mesh to images of unloaded (*left*) and deformed (7% applied tensile strain, *right*) live chondrocytes in agarose using least squares fitting method to compute the strains due to deformation. Scale bar 5 μm.

Chondrocyte Viability

The effect of loading was assessed on chondrocyte viability in the novel construct design. Additional chondrocyte-seeded constructs were cultured to the end of day 14, then on day 15 subjected to the four different mechanical loading regimes (1Hz at 10% compression, 5% tension, 10% shear, and a combination of all three) over 24 hours at 37 ºC/ 5% CO_2, and viability was assessed at the end of the loading period, which was day 16 of culture. Control (unloaded) constructs were also assessed on day 16.

Cell viability was assessed by removing slices from the center of the constructs between the mesh areas, and washing with phosphate buffered saline (PBS, Life Technologies Ltd) before incubation with 5 µM calcein-AM and 1 µM ethidium homodimer-1 (EthD-1) (Life Technologies Ltd) in PBS at 37°C for 20 minutes. The slice was rinsed with PBS before imaging. Cells were viewed on a fluorescent microscope in four fields of view along the slice at 20 X magnification, and the percentage of viable cells were determined. Approximately 120-200 cells were counted per construct.

Statistical Analysis

All experiments were done in triplicate. All data were expressed as the mean ± standard error mean (SEM). Construct strain data were analysed with a linear regression model. Cell viability data were analysed using a one-way ANOVA performed in GraphPad Prism version 8.2.1 (www.graphpad.com). Statistical significance was determined with a p value < 0.05.

Results

Device Accuracy

The mean percentage error at each target movement was < 1.2% both in the parallel (compression and tension) and perpendicular (shear) direction (Table 1). At higher strain percentages, where we have chosen to operate our loading conditions, the error percentage was relatively low. Supplementary figures to show examples of displacement waveform at 1 Hz.

Table 1. Mean (± SEM) percentage error for each target movement of the device in the parallel direction (compression/ tension movement), and perpendicular direction (shear movement). n = 3. Target movement (mm) is distance prescribed to the platen to travel, with the equivalent strain percentage bracketed.

Target movement (mm)	Error per target movement (%)	
	Parallel Direction (Compression/Tension)	Perpendicular Direction (Shear)
0.3 (2%)	0.3 ± 0.3 %	1.2 ± 0.4 %
0.6 (4%)	1.0 ± 0.2 %	0.4 ± 0.2 %
0.9 (6%)	0.03 ± 0.3 %	1.1 ± 0.1 %
1.2 (8%)	0.2 ± 0.3 %	0.4 ± 0.4 %
1.5 (10%)	0.4 ± 0.4 %	0.5 ± 0.3 %
1.8 (12%)	0.3 ± 0.4 %	0.2 ± 0.1 %
2.25 (15%)	0.5 ± 0.6 %	0.1 ± 0.2 %

Cell Viability, Construct and Cellular Strain

Construct Strain

The construct strain analysis technique revealed complex and unique patterns of strain that corresponded to the inhomogeneous nature of cell-seeded agarose constructs (Fig. 4 A, C and E). As the applied strain increased for each of the loading types, the strain within the construct was highest at the mobile end, while the strain within the construct was the lowest at the fixed end. These strains within the constructs were quantified as the average strain percentage along the length of the constructs in the tables in Fig. 4 B, D and F. The average quantified strains within the construct did not equate to the amount of strain applied. Constructs under applied compression showed a linear distribution of strain across the construct (compression with 5%, 10% and 15% applied compression with respective R^2 values of 0.83, 0.93 and 0.89). Constructs with applied tensile and shear strain did not show a linear distribution of strain across the construct (5% and 7% applied tension with R^2 values of 0.58 and 0.75 respectively, 5%, 10% and 15% applied shear strains had R^2 values of 0.31, 0.52 and 0.39 respectively).

Journal of Biomechanical Engineering. Received August 09, 2020;
Accepted manuscript posted May 11, 2021. doi:10.1115/1.4051116

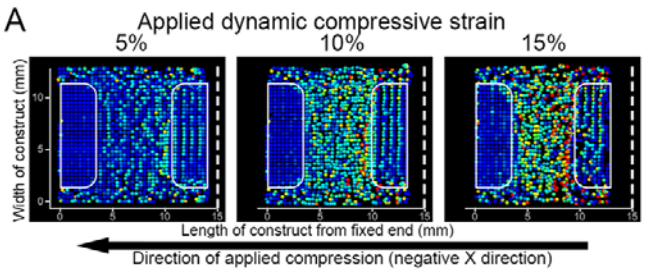

B

Quantified mean strain percentage

Construct length / Applied compressive strain	4 mm	5.5 mm	7 mm	8.5 mm	10 mm
5%	2.4±0.8%	3.0±0.8%	4.2±1.3%	4.7±1.1%	4.8±1.1%
10%	7.1±1.2%	7.9±1.5%	9.6±1.5%	9.8±1.4%	
15%	8.7±1.5%	10.1±1.5%	14.2±1.4%	14.8±1.4%	

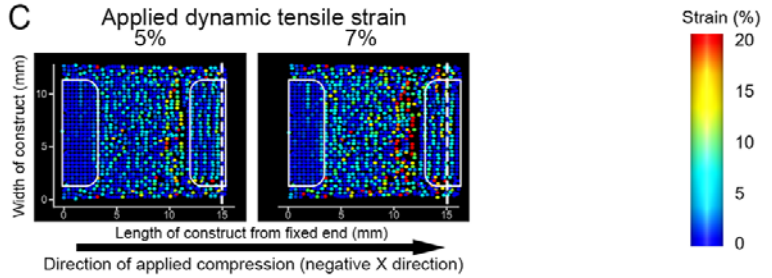

D

Quantified mean strain percentage

Construct length / Applied tensile strain	4 mm	5.5 mm	7 mm	8.5 mm	10 mm	11.5 mm
5%	2.8±0.3%	2.3±0.3%	4.5±1.3%	4.4±0.6%	4.5±1.4%	4.5±1.5%
7%	3.0±0.6%	4.4±0.6%	6.5±0.6%	6.8±1.0%	6.8±1.2%	6.6±1.3%

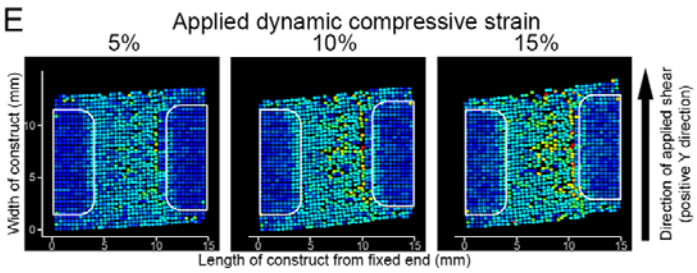

Quantified mean strain percentage

Construct length / Applied shear strain	4 mm	5.5 mm	7 mm	8.5 mm	10 mm
5%	3.1±1.1%	4.2±1.6%	5.1±1.0%	5.7±1.2%	6.5±1.1%
10%	5.0±1.2%	6.2±0.6%	7.6±1.1%	8.8±1.0%	10.4±2.1%
15%	9.7±1.7%	10.2±1.5%	11.2±1.4%	12.8±1.6%	14.8±1.8%

Figure 4. Mean strain distribution images of chondrocyte-seeded agarose constructs at day 14 of culture at 5%, 10% and 15% applied compressive and shear strain (**A** and **E** respectively), and 5% and 7% applied tensile strain (**C**). White dotted-line indicates original length of constructs; white-lined areas indicate the mesh inserts of either side of the construct. Quantified mean strain percentage within the constructs along the length of the construct under applied compressive strain (**B**), tensile strain (**D**) and shear strain (**F**). (N=3 for each strain)

Cell Strain

Processed images of the chondrocytes under applied dynamic loading revealed that the cell shape changed (Fig. 5). Cells under applied dynamic compression became more ellipsoidal perpendicular to the direction of applied compression. Cells under dynamic tensile strain became ellipsoidal in the direction of the applied load, while cells under dynamic shear strain underwent a rotation in the direction of applied load. These shape deformations were used to calculate the surface strain patterns (Fig. 6).

Journal of Biomechanical Engineering. Received August 09, 2020;
Accepted manuscript posted May 11, 2021. doi:10.1115/1.4051116

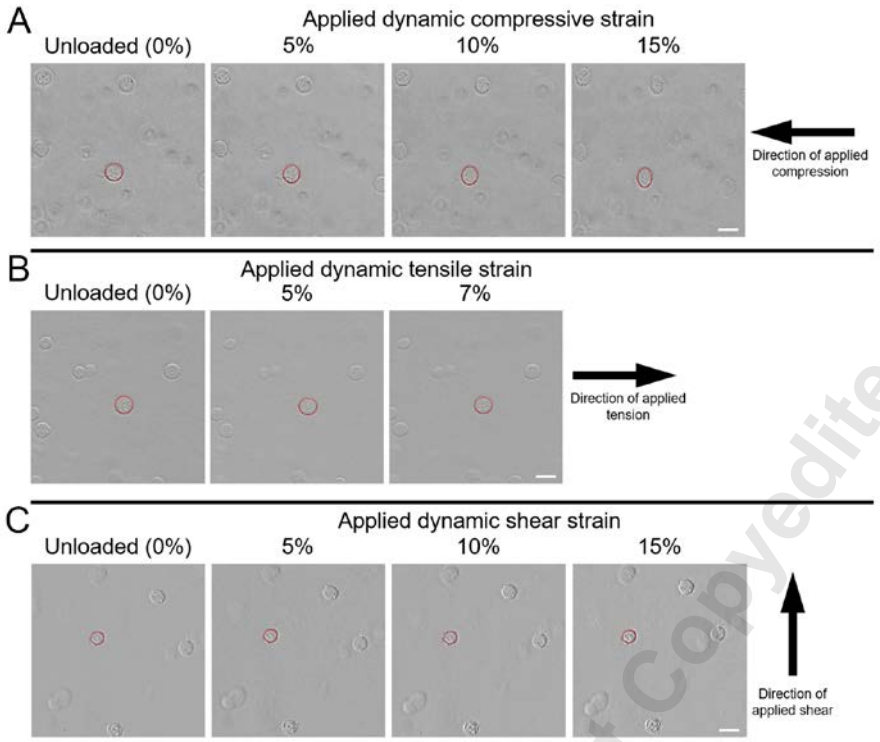

Figure 5. Representative images of chondrocytes in constructs (post image processing in ImageJ) under (**A**) unloaded, 5%, 10% and 15% applied dynamic compressive strain, (**B**) unloaded, 5% and 7% applied tensile strain, and **(C) unloaded, 5%, 10% and 15% shear strain.** Examples of the cells and their deformation under applied strain are outlined in red. Arrows indicate direction of applied strain load. Scale bar is 10 μm.

The surface strain distribution patterns of the cells were heterogeneous. They revealed regions within the cell with higher strains than others, for example, cells under dynamic compression load had higher strain regions on the side of the mobile end.

The *in situ* model showed that the development of peak surface strain within the cells was more prominent in tension and compression loads than under shear. Moreover, heterogeneous strain distribution was dependent on the original cell shape as well as the mode of strain applied, indicating that the complex interplay between cell shape and the type of mechanical stimuli exists in the development of the overall cell strain patterns.

Journal of Biomechanical Engineering. Received August 09, 2020;
Accepted manuscript posted May 11, 2021. doi:10.1115/1.4051116

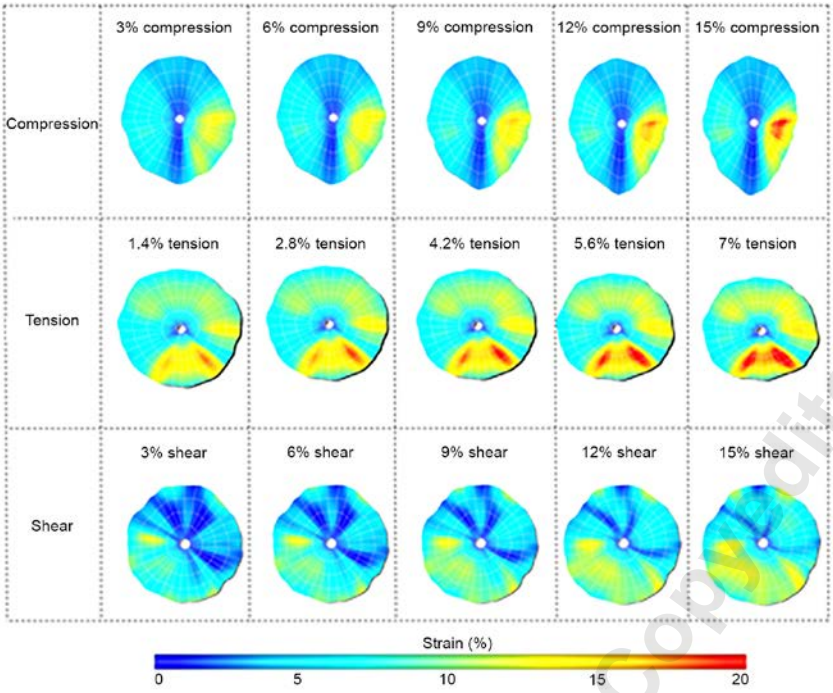

Figure 6. Representative images of cell surface strain calculated under compression, tension, and shear deformation. The pattern developed on the cell surface is dependent both on mode of application as well as the original cell shape.

Cell Viability

Chondrocyte viability was maintained above 88% for all conditions, with no statistically significant differences between strained cells and control (unloaded) constructs cultured for 14 days, followed by a 24 hr mechanical loading period, Table 2.

Table 2. Percentage cell viability within constructs subjected to different loading regimes. Each value represents mean ± SEM. At least 100 cells were measured from each condition (N = 3).

Loading Regime	Viability (%)
Control	92 ± 2
Compression	89 ± 2
Tension	88 ± 1
Shear	89 ± 2
Combination	90 ± 2

Discussion

The device that we have developed accurately applies dynamic compression, tension and shear strains to 3D hydrogel constructs. Given the importance of delivering well defined strains to the relatively small constructs, we used two precision-made commercial actuators for axial and shear motions. Linear actuators are one of the most commonly used instruments for accurate positioning (and in commercial devices such as BioSyntech, QC.). High accuracy was achieved by a stepper motor with a fine pitch lead screw, appropriate maximum force and motor speed. Only a handful of previous studies have provided a system for accurate application of complex mechanical deformation on constructs that includes compression,

tension, and shear. The direct contribution of the applied shear load is not easily quantifiable in rotating culture bioreactors [28], where cell-seeded scaffolds are exposed to complex mechanical loading patterns incorporating fluid-induced shear. Mechanical loading devices on 3D culture systems that involves a moving arm against a stationary part, such as tribology (sliding indentation) devices [29,30], and tensile loading devices [31], inherently result in a non-homogeneous strain distribution through the constructs, and therefore an applied strain gradient on the seeded cells within. This inherent characteristic of the strain distribution makes it difficult to understand the effect of strain on cells. It is important to minimise the gradient strain effect and characterise the strain cells experience in order to be able to interpret the effect of the strain on the cells.

The control system of our device enables a wide range of loading regimes to be implemented due to the customisable macro. This enables different types and combinations of mechanical effects on chondrocytes to be investigated, enabling abnormal, such as 0.5 Hz loading frequency, and physiological normal, such as 1 Hz loading frequency, conditions to be investigated.

Chondrocytes seeded in agarose gels have been extensively used to study the influence of compressive strain on the metabolism of chondrocytes [9,32–35]. This *in vitro* model system provides mechanical stability, reproducibility and allows the application of physiological or abnormal gait types of strain. However, agarose is inherently viscoelastic. Therefore, it was necessary to design an appropriate construct and gripping mechanism in order to apply dynamic strain. Other studies have employed a vertical platen on top of chondrocyte-agarose constructs to apply dynamic compressive loading [36]. However, due to the inherent nature of hydrogels to stress-relax [37,38], and the ability to apply dynamic compressive, tensile and shear strains in combination while having the ability to visualise cell deformation for cellular strain analysis, our system utilised a horizontal loading design.

Horizontal loading platens have often used sintered glass endplates infiltrated with agarose gel to allow for gripping during the application of dynamic compression [39,40]. Our preliminary approach also tested sintered glass but found that constructs could not withstand applied tensile load and caused the hydrogel to detach from the porous endplates. As a result, we developed a mesh interface which maintained the construct integrity during mechanical loading, and reduced hydrogel compaction over the course of loading. The strain applied to the constructs correlates to the cellular strain within the hydrogel, with cells stretched up to 7% elongation.

For long term culture experiments, it is essential to maintain cell viability, and the potential for active metabolism of cell seeded constructs within a culture system as loading regimes may alter transport of metabolites into the constructs [41]. In our device, chondrocyte viability was maintained above 88% for all test conditions within the construct for up to 15 days.

These data suggest that the culture conditions, the materials used in the device and the applied loading regimes did not affect cell viability or mechanical integrity of the constructs.

The system also enables eight constructs in separate wells of the culture plate to be simultaneously tested, providing sufficient replicates for each experiment. In this study, we have used either side of the device to apply different mechanical strain simultaneously. Having multiple samples allow for unforeseen failure of constructs and would not compromise the entire experiment, as opposed to bioreactors in which the samples are all contained within the same culture chamber [39]. The number of samples per experiment also allows for more than one assay to be performed from one loading experiment, samples can be allocated for viability assessment, RNA extraction and fixed for histology. Due to the size of the construct, it contains sufficient cells for good RNA yields. One of the major strengths of our system is the ability to characterize cell deformation patterns under different types of strains. Internal strain distribution patterns in chondrocytes after mechanical loading was heterogeneous, displaying peak strains within different regions of the cells. Many studies assess cell deformation by measuring aspect ratio changes [35,40,42]. Although such studies have been instrumental in analysing the role of mechanical loading at the whole cell level, our results indicate that aspect ratio change alone may not reveal the full effects of cell deformation. Our system can perform more detailed analysis and show regional variations in strains within the cells, which might be crucial in identifying mechanotransduction pathways in chondrocytes [43,44].

We have also identified some limitations of our device. Firstly, devices using a platen for the application of load have an inherent limitation as it creates an inhomogeneous loading environment. The side of the construct closest to the platen is exposed to higher strains than the static side, as we have identified with our strain maps, consequently causing a strain gradient across the construct. This may affect downstream analysis, such as RNA analysis, where the entire construct is homogenised for RNA extraction, therefore making it impossible to differentiate how changes in magnitudes of strain affect cellular activity. However, our construct was designed to minimise this effect by sampling the centre part of the construct for downstream analysis. This minimises the range of strain gradients across the construct for a more accurate downstream analysis. Secondly, although the image acquisition and processing parts of our system are relatively streamlined, considerable manual processing is required. To migrate this process to a high-throughput system that can analyse a large number of datasets, a machine-learning based approach will enable many of these processes to be automated.

In conclusion, we have developed a novel system that can apply a range of mechanical loads to 3D constructs containing chondrocytes in physiologically relevant strains and frequencies and compute cellular strains under these complex mechanical stimulations. A 3D hydrogel construct has also been successfully designed to withstand long term compressive,

tensile, and shear loading. The features of our system, and those of the construct, will enable a deeper understanding of the chondrocyte mechanobiology.

References

[1] Sah, R. L.-Y., Kim, Y.-J., Doong, J.-Y. H., Grodzinsky, A. J., Plass, A. H. K., and Sandy, J. D., 1989, "Biosynthetic response of cartilage explants to dynamic compression," J. Orthop. Res., **7**(5), pp. 619–636.

[2] Grodzinsky, A. J., Levenston, M. E., Jin, M., and Frank, E. H., 2000, "Cartilage tissue remodeling in response to mechanical forces," Annu. Rev. Biomed. Eng., **2**, pp. 691–713.

[3] Carter, D. R., Beaupre, G. S., Wong, M., Smith, R. L., Andriacchi, T. P., and Schurman, D. J., 2004, "The mechanobiology of articular cartilage development and degeneration," Clin Orthop Relat Res, (427), pp. 69–77.

[4] Emans, P. J., and Peterson, L., 2014, Developing insights in cartilage repair, Springer.

[5] Chan, D. D., Cai, L., Butz, K. D., Trippel, S. B., Nauman, E. A., and Neu, C. P., 2016, "In vivo articular cartilage deformation: Noninvasive quantification of intratissue strain during joint contact in the human knee," Sci. Rep., **6**, pp. 1–14.

[6] Bleuel, J., Zaucke, F., Brüggemann, G.-P., and Niehoff, A., 2015, "Effects of cyclic tensile strain on chondrocyte metabolism: A systematic review," PLoS One, **10**(3), pp. 1–15.

[7] Bian, L., Fong, J. V., Lima, E. G., Stoker, A. M., Ateshian, G. A., Cook, J. L., and Hung, C. T., 2010, "Dynamic Mechanical Loading Enchances Functional Properties of Tissue-Engineerd Cartilage Using Mature Canine Chondrocytes," Tissue Eng. Part A, **16**(5), pp. 17–20.

[8] Lee, D. a, and Bader, D. L., 1997, "Compressive strains at physiological frequencies influence the metabolism of chondrocytes seeded in agarose.," J. Orthop. Res., **15**(2), pp. 181–8.

[9] Mauck, R. L., Soltz, M. A., Wang, C. C. B., Wong, D. D., Chao, P. G., and Ateshian, G. A., 2000, "Functional Tissue Engineering of Articular Cartilage Through Dynamic Loading of Chondrocyte-Seeded Agarose Gels," J. Biomech. Eng., **122**, pp. 252–260.

[10] Appelman, T. P., Mizrahi, J., Elisseeff, J. H., and Seliktar, D., 2011, "The influence of biological motifs and dynamic mechanical stimulation in hydrogel scaffold systems on the phenotype of chondrocytes," Biomaterials, **32**(6), pp. 1508–1516.

[11] Becker, J. L., Prewett, T. L., Spaulding, G. F., and Goodwin, T. J., 2004, "Three-Dimensional Growth and Differentiation of Ovarian Tumor Cell Line in High Aspect Rotating-Wall Vessel: Morphologic and Embryologic Considerations," J. Cell. Biochem., **51**(3), pp. 283–289.

[12] Waldman, S. D., Spiteri, C. G., Grynpas, M. D., Pilliar, R. M., and Kandel, R. a, 2003, "Long-term intermittent shear deformation improves the quality of cartilaginous tissue formed in vitro.," J. Orthop. Res., **21**(4), pp. 590–6.

[13] Fitzgerald, J. B., Jin, M., Chai, D. H., Siparsky, P., Fanning, P., and Grodzinsky, A. J., 2008, "Shear- and compression-induced chondrocyte transcription requires MAPK activation in cartilage explants.," J. Biol. Chem., **283**(11), pp. 6735–43.

[14] Pingguan-Murphy, B., and Nawi, I., 2012, "Upregulation of matrix synthesis in chondrocyte-seeded agarose following sustained bi-axial cyclic loading," Clinics, **67**(8), pp. 939–944.

[15] Wang, N., Grad, S., Stoddart, M. J., Niemeyer, P., Reising, K., Schmal, H., S??dkamp, N. P., Alini, M., and Salzmann, G. M., 2014, "Particulate cartilage under bioreactor-induced compression and shear," Int. Orthop., **38**(5), pp. 1105–1111.

[16] Di Federico, E., Shelton, J. C., and Bader, D. L., 2017, "Complex mechanical conditioning of cell-seeded agarose constructs can influence chondrocyte biosynthetic activity," Biotechnol. Bioeng., **114**(7), pp. 1614–1625.

[17] Kelly, P. a, and O'Connor, J. J., 1996, "Transmission of rapidly applied loads through articular cartilage. Part 2:

Cracked cartilage.," Proc. Inst. Mech. Eng. H., **210**(C), pp. 39–49.

[18] Vanderploeg, E. J., Imler, S. M., Brodkin, K. R., García, A. J., and Levenston, M. E., 2004, "Oscillatory tension differentially modulates matrix metabolism and cytoskeletal organization in chondrocytes and fibrochondrocytes," J. Biomech., **37**(12), pp. 1941–1952.

[19] Huang, J., Ballou, L. R., and Hasty, K. A., 2007, "Cyclic equibiaxial tensile strain induces both anabolic and catabolic responses in articular chondrocytes," Gene, **404**(1–2), pp. 101–109.

[20] Wong, M., and Carter, D. R., 2003, "Articular cartilage functional histomorphology and mechanobiology: a research perspective," Bone, **33**(1), pp. 1–13.

[21] Nicodemus, G. D., and Bryant, S. J., 2008, "The role of hydrogel structure and dynamic loading on chondrocyte gene expression and matrix formation," J. Biomech., **41**(7), pp. 1528–1536.

[22] van Beuningen, H. M., Stoop, R., Buma, P., Takahashi, N., van der Kraan, P. M., and van den Berg, W. B., 2002, "Phenotypic differences in murine chondrocyte cell lines derived from mature articular cartilage," Osteoarthr. Cartil., **10**(12), pp. 977–986.

[23] Leung, S., McGlashan, S. R., Musson, D. S. P., Cornish, J., Anderson, I. A., and Shim, V. B. K., 2018, "Investigations of Strain Fields in 3D Hydrogels Under Dynamic Confined Loading," J. Med. Biol. Eng., **38**(3), pp. 514–522.

[24] Malcolm, D. T. K., Nielsen, P. M. F., Hunter, P. J., and Charette, P. G., 2002, "Strain measurement in biaxially loaded inhomogeneous, anisotropic elastic membranes," Biomech. Model. Mechanobiol., **1**(3), pp. 197–210.

[25] Parker, M. D., Azhar, M., Babarenda Gamage, T. P., Alvares, D., Taberner, A. J., and Nielsen, P. M. F., 2012, "Surface deformation tracking of a silicone gel skin phantom in response to normal indentation," Engineering in Medicine and Biology Society (EMBS) Proceedings of the 34th Annual International Conference of the IEEE, San Diego, California USA, pp. 527–530.

[26] Kim, J. J., Musson, D., Mathews, B., Cornish, J., Anderson, I., and Shim, V. B., 2016, "Applying physiologically relevant strains to tenocytes in an in-vitro cell device induces in-vivo like behaviours," ASME J. Biomech. Eng., **138**(12), pp. 1–9.

[27] Shim, V. B., Besier, T. F., Lloyd, D. G., Mithraratne, K., and Fernandez, J. F., 2016, "The influence and biomechanical role of cartilage split line pattern on tibiofemoral cartilage stress distribution during the stance phase of gait," Biomech. Model. Mechanobiol., **15**(1), pp. 195–204.

[28] Wimmer., M. A., Grad., S., Kaup, T. M., Hänni, M., Schneider, E., Gogolewski, S., and Alini, M., 2004, "Tribology Approach to the Engineering and Study of Articular Cartilage," Tissue Eng., **10**(9), pp. 1436–1445.

[29] Khoshgoftar, M., van Donkelaar, C. C., and Ito, K., 2011, "Mechanical stimulation to stimulate formation of a physiological collagen architecture in tissue- engineered cartilage: a numerical study," Comput. Methods Biomech. Biomed. Engin., **14**(2), pp. 135–144.

[30] Kock, L. M., Ito, K., and van Donkelaar, C. C., 2013, "Sliding indentation enhances collagen content and depth-dependent matrix distribution in tissue-engineered cartilage constructs.," Tissue Eng. Part A, **19**(17–18), pp. 1949–59.

[31] Connelly, J. T., Vanderploeg, E. J., and Levenston, M. E., 2004, "The influence of cyclic tension amplitude on chondrocyte matrix synthesis: Experimental and finite element analyses," Biorheology, **41**(3–4), pp. 377–387.

[32] Buschmann, M. D., Gluzband, Y. A., Grodzinsky, A. J., and Hunziker, E. B., 1995, "Mechanical compression modulates matrix biosynthesis in chondrocyte/agarose culture," J. Cell Sci., **108**, pp. 1497–1508.

[33] Buschmann, M. D., Gluzband, Y. A., Grodzinsky, A. J., Kimura, J. H., and Hunziker, E. B., 1992, "Chondrocytes in agarose culture synthesize a mechanically functional extracellular matrix," J Orthop Res, **10**(6), pp. 745–758.

[34] Knight, M. M., Ghori, S. A., Lee, D. A., and Bader, D. L., 1998, "Measurement of the deformation of isolated chondrocytes in agarose subjected to cyclic compression," Med. Eng. Phys., **20**(9), pp. 684–688.

[35] Lee, D. A., Knight, M. M., F Bolton, J., Idowu, B. D., Kayser, M. V, and Bader, D. L., 2000, "Chondrocyte

deformation within compressed agarose constructs at the cellular and sub-cellular levels," J. Biomech., **33**(1), pp. 81–95.

[36] Di Federico, E., Bader, D. L., and Shelton, J. C., 2014, "Design and validation of an in vitro loading system for the combined application of cyclic compression and shear to 3D chondrocytes-seeded agarose constructs," Med. Eng. Phys., **36**(4), pp. 534–540.

[37] Mitchell, J. R., 1980, "Rheology of gels," J. Texture Stud., **11**, pp. 315–337.

[38] Anseth, K. S., Bowman, C. N., and Brannon-Peppas, L., 1996, "Mechanical properties of hydrogels and their experimental determination," Biomaterials, **17**(17), pp. 1647–1657.

[39] Yusoff, N., Abu Osman, N. A., and Pingguan-Murphy, B., 2011, "Design and validation of a bi-axial loading bioreactor for mechanical stimulation of engineered cartilage," Med. Eng. Phys., **33**(6), pp. 782–788.

[40] Sawae, Y., Shelton, J. C., Bader, D. L., and Knight, M. M., 2004, "Confocal analysis of local and cellular strains in chondrocyte-agarose constructs subjected to mechanical shear," Ann. Biomed. Eng., **32**(6), pp. 860–870.

[41] Wilkins, R. J., Browning, J. A., and Ellory, J. C., 2000, "Topical Review Surviving in a Matrix: Membrane Transport in Articular Chondrocytes," J. Membr. Biol., **177**, pp. 95–108.

[42] Lee, D. A., and Bader, D. L., 1995, "The development and characterization of anin vitro system to study strain-induced cell deformation in isolated chondrocytes," Vitr. Cell. Dev. Biol. - Anim., **31**(11), pp. 828–835.

[43] Kääb, M. J., Richards, R. G., Ito, K., ap Gwynn, I., and Nötzli, H. P., 2003, "Deformation of Chondrocytes in Articular Cartilage under Compressive Load: A Morphological Study," Cells Tissues Organs, **175**(3), pp. 133–139.

[44] Di Federico, E., Bader, D. L., and Shelton, J. C., 2020, "3D models of chondrocytes within biomimetic scaffolds: Effects of cell deformation from loading regimens," Clin. Biomech., (July 2019), pp. 1–10.

Supplementary

Supplementary details on device and construct optimization, validation and cell viability methods are provided by the following.

Positions along the loading platens of the device were measured by the laser displacement meter, as shown in Fig. S 1. These positions correlate with where samples will be attached. The mean percentage error at each position corresponding to for each target movement was lower than 1.5% in both the parallel (compression and tension) and perpendicular (shear) direction (Table S 1).

Journal of Biomechanical Engineering. Received August 09, 2020;
Accepted manuscript posted May 11, 2021. doi:10.1115/1.4051116

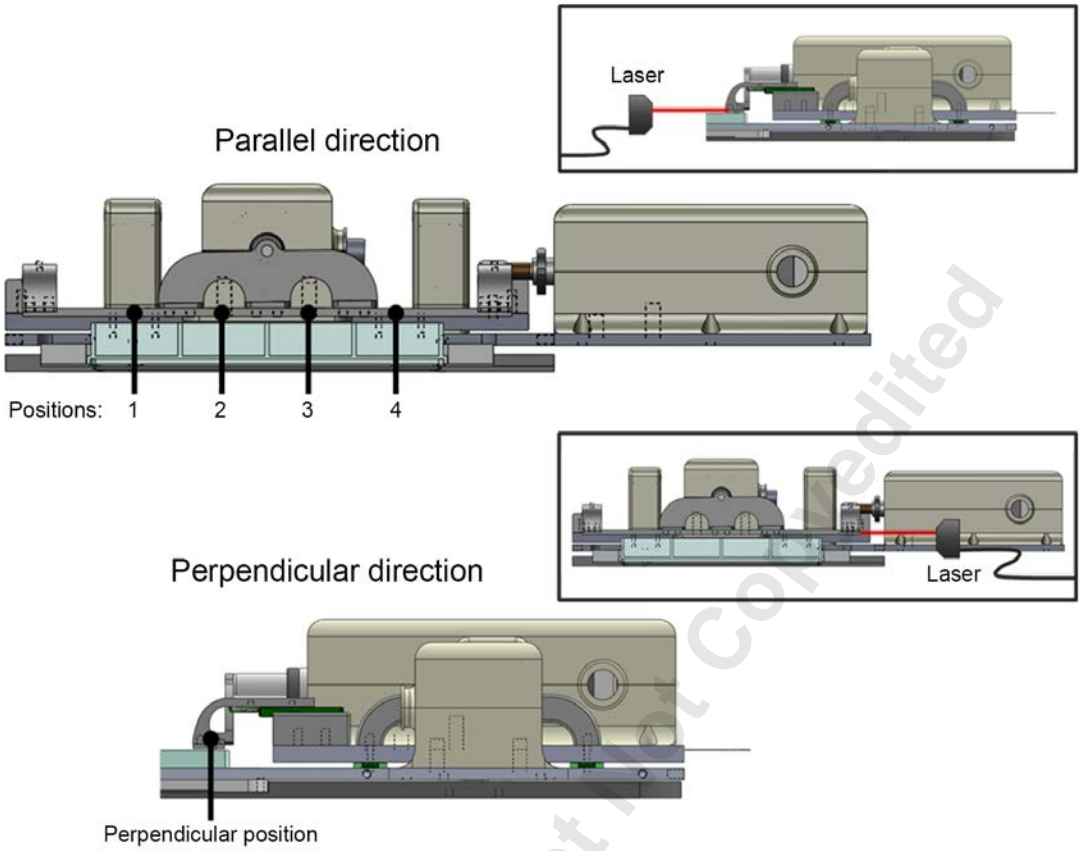

Figure S1 Schematics of where the positions were measured in the parallel direction (*top*) and in the perpendicular direction (*bottom*). Inserts show where the laser was set up for each position measurement.

Table S1. Mean error percentage at each position for the target movement of the device in the parallel direction (compression/ tension movement), and perpendicular direction (shear movement). Each movement was measured three times.

Target movement (mm)	Error per target movement				
	Parallel Direction (Compression/Tension)				Perpendicular (Shear)
	Position 1	Position 2	Position 3	Position 4	
0.3	0.6 ± 0.1 %	0.3 ± 0.4 %	0.7 ± 0.2 %	0.8 ± 0.4 %	1.2± 0.4 %
0.6	1.0 ± 0.1 %	1.0± 0.2 %	0.6 ± 0.2 %	0.1 ± 0.1 %	0.4 ± 0.2 %
0.9	0.3 ± 0.03 %	0.3 ± 0.1 %	0.3 ± 0.1 %	1.0 ± 0.2 %	1.1 ± 0.1 %
1.2	0.1 ± 0.1 %	0.7 ± 0.3 %	0.6± 0.4 %	0.9 ± 0.3 %	0.4 ± 0.4 %
1.5	0.6 ± 0.1 %	0.8 ± 0.01 %	0.8 ± 0.3 %	0.4 ± 0.3 %	0.5 ± 0.3 %
1.8	1.0 ± 0.1 %	0.7 ± 0.2 %	0.8 ± 0.4 %	0.2 ± 0.2 %	0.2 ± 0.1 %
2.25	1.0 ± 0.1 %	1.0 ± 0.4 %	0.7 ± 0.1 %	1.2 ± 0.2 %	0.1 ± 0.2 %

Construct optimization:

The geometry of the cell-hydrogel construct was governed by the 8-rectangular-well plastic culture plates. Constructs were designed in a rectangular shape because it provided a more uniform application of tensile strain as validated by Kim, *et al* [26]. The construct was designed to incorporate a gap between the hydrogel and the bottom of the culture plate to ensure

Journal of Biomechanical Engineering. Received August 09, 2020;
Accepted manuscript posted May 11, 2021. doi:10.1115/1.4051116

media was able to cover the whole sample during culture and dynamic loading. The mesh size was optimized to ensure the hydrogel would sufficiently infiltrate into and bond to the mesh so that the largest magnitude of tensile strain could be applied. Various mesh sizes (wire diameter, and porosity, Fig. S 2) were tested in various layering configurations. Three samples were prepared for each configuration. Agarose was set between two ends and tensile strain was applied to each combination after 14 days incubation in PBS. Mean percentage of elongation before breakage of each configuration is recorded in the table in Fig. S 2.

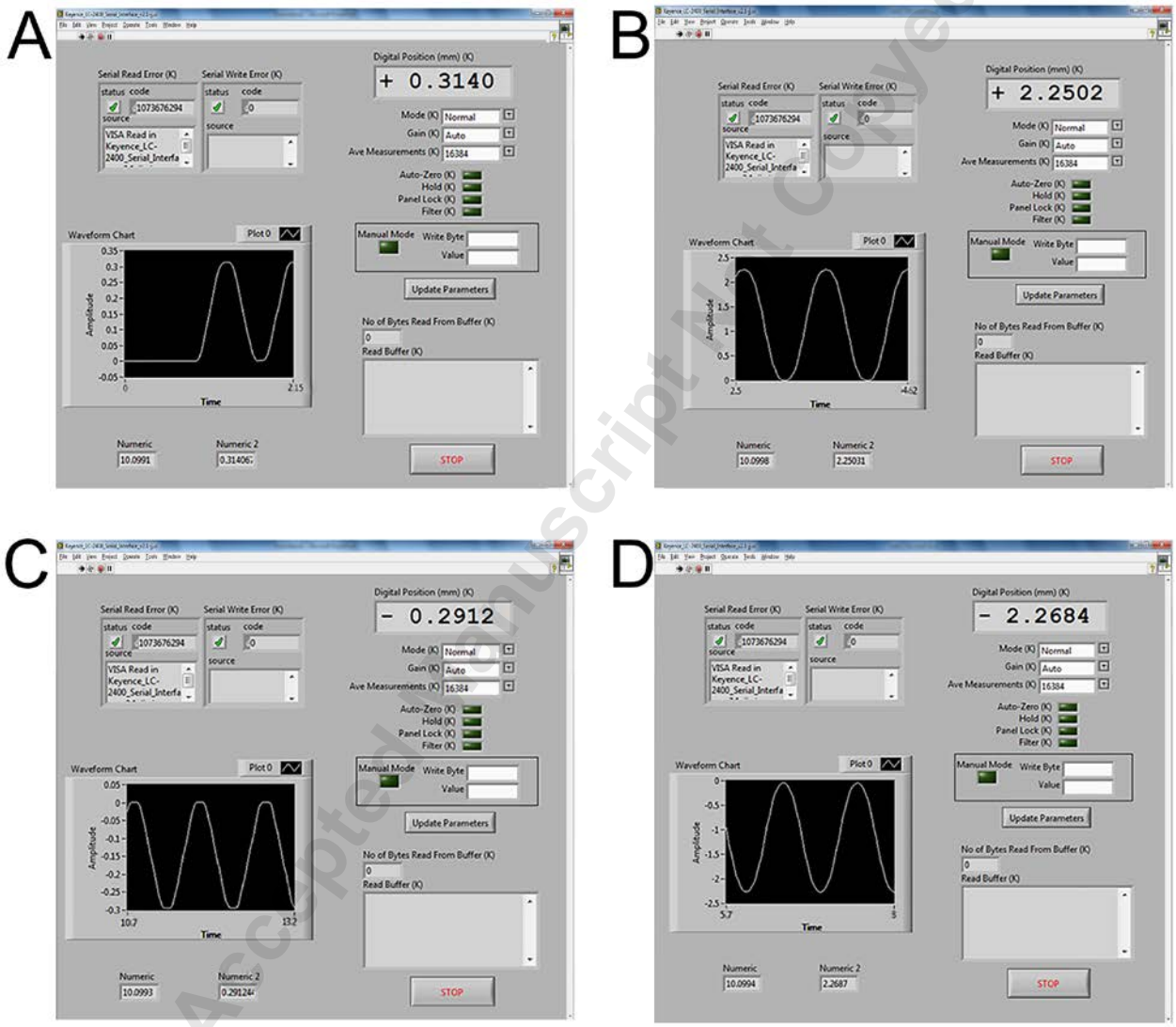

Figure S2. Representative wave forms of parallel direction platen displacement at 1 Hz with (A) 0.3 mm target (2%, including from start-up) and (B) 2.25 mm target (15%). Perpendicular platen displacement at 1 Hz with (C) 0.3 mm target (2% strain) and (D) 2.25 mm (15%). Digital position indicates actual platen movement. Time domain is in seconds.

Journal of Biomechanical Engineering. Received August 09, 2020;
Accepted manuscript posted May 11, 2021. doi:10.1115/1.4051116

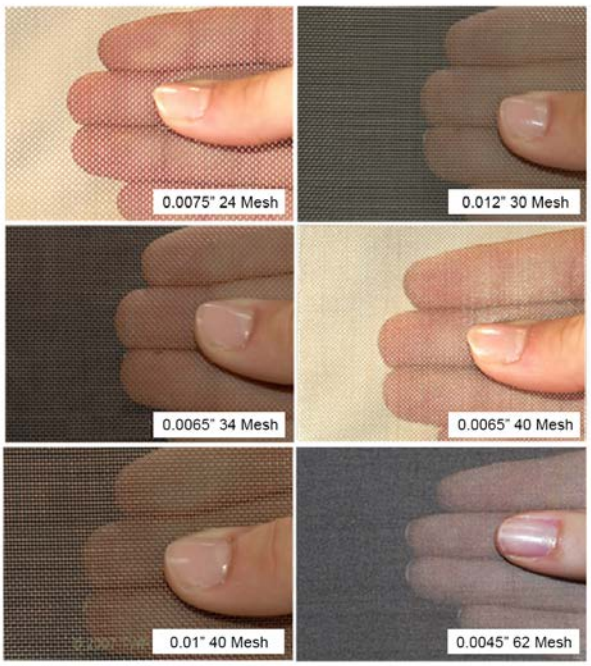

Mesh size	Configuration (layers of mesh)	Mean % of elongation before breakage ± SEM
24 Mesh 0.0075"	3	12 ± 4.4%
30 Mesh 0.012"	2	9 ± 4.2%
30 Mesh 0.012"	3	5 ± 1.3%
34 Mesh 0.065"	3	9 ± 0.75
40 Mesh 0.0065"	3	7 ± 4.2%
40 Mesh 0.0065"	5	6 ± 1.4%
40 Mesh 0.01"	3	5 ± 1.0%
62 Mesh 0.0045"	3	8 ± 1.7%
62 Mesh 0.0045"	6	7 ± 2.4%

Figure S3. Sample images obtained from TWP Inc. show the different sizes of the wire diameter and porosity for each mesh tested. Table is the mean elongation percentage of each mesh size and layering configuration. First number denotes porosity of mesh in opening percentage. Second number denotes wire diameter in inches.

Cell Viability

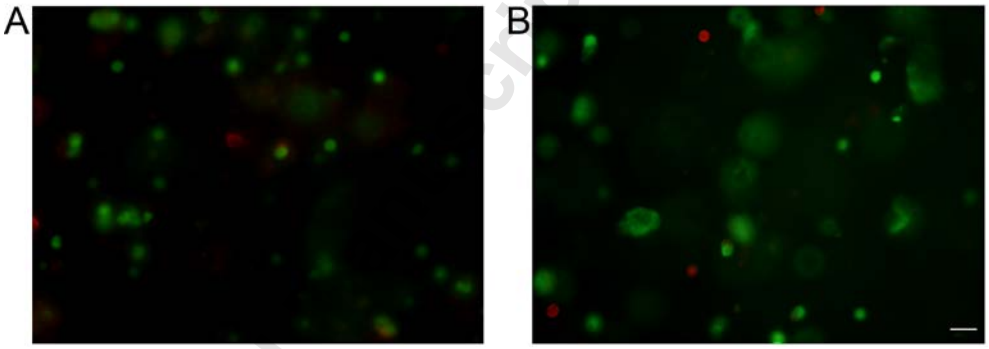

Figure S4 Representative images of live (green)/dead (red) stain of encapsulated chondrocytes in middle section of constructs: (A) control on day 16; (B) after 24 hours of combination strain loading. Scale bar 20 μm

List of Table Captions

Table 1. Mean (± SEM) percentage error for each target movement of the device in the parallel direction (compression/ tension movement), and perpendicular direction (shear movement). n = 3. Target movement (mm) is distance prescribed to the platen to travel, with the equivalent strain percentage bracketed.

Table 2. Percentage cell viability within constructs subjected to different loading regimes. Each value represents mean ± SEM. At least 100 cells were measured from each condition (N = 3).

Table S1. Mean error percentage at each position for the target movement of the device in the parallel direction (compression/ tension movement), and perpendicular direction (shear movement). Each movement was measured three times.

List of Figure Captions

Figure 1. Schematic of assembled device in (**A**) side and (**B**) plan view. The side view shows the device in the raised state. Thick black arrows indicate actuators movement direction to apply (i) compressive, (ii) tensile and (iii) shear strains.

Figure 2. (**A**) Side view of assembled construct in (*left*) schematic and (*right*) image. (**B**) Samples attached to the device in (*left*) schematic and (*right)* image.

Figure 3. Representative of fitting a mesh to images of unloaded (left) and deformed (7% applied tensile strain, right) live chondrocytes in agarose using least squares fitting method to compute the strains due to deformation. Scale bar 5 μm.

Figure 4. Mean strain distribution images of chondrocyte-seeded agarose constructs at day 14 of culture at 5%, 10% and 15% applied compressive and shear strain (**A** and **E** respectively), and 5% and 7% applied tensile strain (**C**). White dotted-line indicates original length of constructs; white-lined areas indicate the mesh inserts of either side of the construct. Quantified mean strain percentage within the constructs along the length of the construct under applied compressive strain (**B**), tensile strain (**D**) and shear strain (**F**). (N=3 for each strain)

Figure 5. Representative images of chondrocytes in constructs (post image processing in ImageJ) under (**A**) unloaded, 5%, 10% and 15% applied dynamic compressive strain, (**B**) unloaded, 5% and 7% applied tensile strain, and (**C**) unloaded, 5%, 10% and 15% shear strain. Examples of the cells and their deformation under applied strain are outlined in red. Arrows indicate direction of applied strain load. Scale bar is 10 μm.

Figure 6. Representative images of cell surface strain calculated under compression, tension, and shear deformation. The pattern developed on the cell surface is dependent both on mode of application as well as the original cell shape.

Figure S1. Schematics of where the positions were measured in the parallel direction (*top*) and in the perpendicular direction (*bottom*). Inserts show where the laser was set up for each position measurement.

Figure S2. Representative wave forms of parallel direction platen displacement at 1 Hz with (A) 0.3 mm target (2%, including from start-up) and (B) 2.25 mm target (15%). Perpendicular platen displacement at 1 Hz with (C) 0.3 mm target (2% strain) and (D) 2.25 mm (15%). Digital position indicates actual platen movement. Time domain is in seconds.

Figure S3. Sample images obtained from TWP Inc. show the different sizes of the wire diameter and porosity for each mesh tested. Table is the mean elongation percentage of each mesh size and layering configuration. First number denotes porosity of mesh in opening percentage. Second number denotes wire diameter in inches.

Figure S5 Representative images of live (green)/dead (red) stain of encapsulated chondrocytes in middle section of constructs: (A) control on day 16; (B) after 24 hours of combination strain loading. Scale bar 20 μm